

Geologically consistent multiphysics imaging of the Darajat geothermal steam field

Wolfgang Soyer^{1*}, Randall Mackie¹, Stephen Hallinan¹, Alice Pavesi¹, Gregg Nordquist², Aquaredi Suminar³, Rindu Intani³ and Chris Nelson³ present a joint 3D inversion workflow, incorporating the production field model as a structural reference in order to derive mutually consistent subsurface resistivity, density and velocity distributions, as well as relocated MEQ events.

Introduction

Darajat is a vapor-dominated, producing geothermal field in West Java, Indonesia. Located along a range of Quaternary volcanic centres, it is associated with an eroded andesitic stratovolcano, and its reservoir is predominantly comprised of thick lava flows and intrusions in a stratovolcano central facies (Rejeki et al., 2010). First production from the field was started in 1994 with the installation of a 55 MW plant, and capacity was added in 2000 and 2007 to bring the total to 271 MW.

Several ground geophysics data sets have been acquired during successive surveys – including gravity and magnetotelluric (MT) surveys, and continuing micro-earthquake (MEQ) monitoring (Soyer et al., 2017). While each survey was independently modelled and interpreted, a quantitatively integrated 3D inversion modelling study had not been undertaken. We present a joint 3D inversion workflow, incorporating the production field model as a structural reference in order to derive mutually consistent subsurface resistivity, density and velocity distributions, as well as relocated MEQ events.

Magnetotelluric measurements — an inductive EM technique most sensitive to conductors — are of particular value in volcanic-hosted, high-enthalpy geothermal exploration. The hydrothermal mineral alteration grade varies with temperature, and the low-temperature (<180°C) clay zones above and flanking the reservoir are electrically very conductive with respect to the higher-grade

(>225°C) propylitic alteration assemblages at reservoir temperatures (e.g. Ussher et al., 2000; Cumming, 2009; Trainor-Guitton et al., 2014). Where the field is in equilibrium the alteration facies can thus be used as a geothermometer, and an accurate 3D model of electrical resistivity images the geothermal reservoir structure. Gravity relates linearly to bulk density, which is primarily a function of a lithological unit's rock matrix density and porosity. The gravity data provide a constraint on the basement structure and depths. The positioning of MEQ events in time and space gives indications on the stress regime evolution, and possibly fluid paths if related to active fractures (Pramono and Colombo, 2005; Perdana and Nelson, 2014). The related velocity tomographic inversion modelling provides Vp and Vs volumes that are in turn related to lithology, porosity and effective fluid phase differences (e.g. steam zone saturation vs liquid-dominated zone below).

Geophysical datasets

The MT dataset comprises 85 soundings from surveys in 1996 and 2004 (Figure 1) covering a frequency range from nominally 0.001 to 100 and 10,000 Hz respectively. Gravity was measured in 1996 over a much wider area, with closer and more regular spacing in the production area, and a subset of 540 measurements from the central area was used in the modelling here. The MEQ data includes 6100 handpicked Vp and Vs arrival times, recorded at 21 receiver positions, during acquisition periods from 2006 to 2015

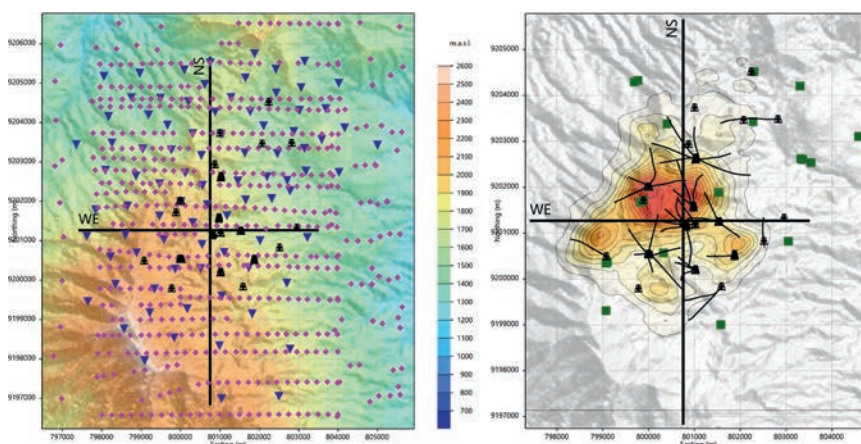


Figure 1 Locations of geophysical data at Darajat: MT (blue), gravity (violet), and MEQ receivers (green). Wells and their trajectories are shown in black. The MEQ event distribution is shown as a 'heat map' on the right.

¹ CGG Multi-Physics | ² Consultant | ³ Star Energy Geothermal

* Corresponding author, E-mail: wolfgang.soyer@cgg.com

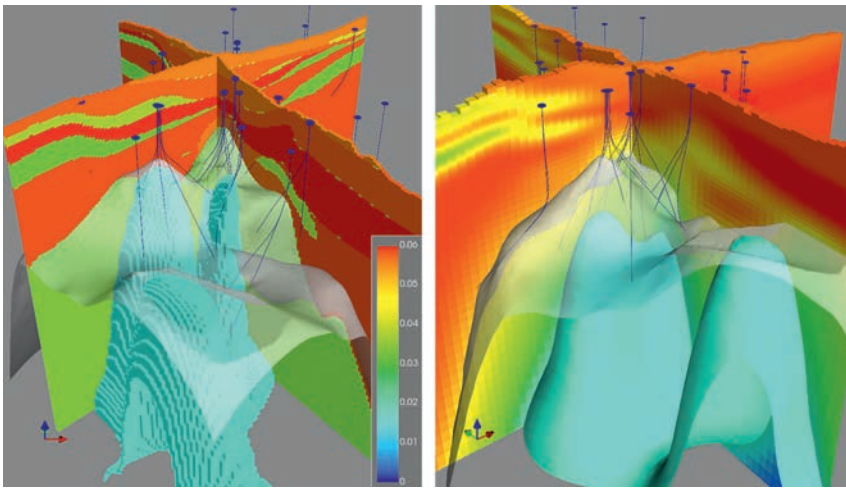


Figure 2 3D porosity reference model. Left: original concept model. Right: resampled on to the geophysics 3D inversion mesh, extrapolated and filtered, for use as structural reference model in joint 3D inversions. Units in volume fraction (0.01 is 1% porosity). The transparent surface marks the estimated top of the petrophysical grouping of lava flows (andesite, basalt and autoclastic breccia) from the geological model. Poorly constrained (few drill intersections) low-porosity microdiorite pillars are shown in light blue.

(Figure 1). The MEQ data were recorded with three-component sensors buried about 1 m below the surface (Perdana and Nelson, 2014). Observed microseismic activity is primarily induced from injection of condensate through a few injection wells. Initial event locations were estimated from 1D modelling of P-wave velocity.

Geological and porosity models

Darajat is part of an older andesitic stratovolcano complex that has collapsed and eroded. The lower reservoir zone is characterized by thick lavas and intrusions of a central volcanic facies type, surrounded by pyroclastic margins of proximal-medial facies. Above are younger volcanics of different lithologies from later eruptions.

A geological model had been generated for the Darajat field based on a wide range of input data: drill core, cutting and surface sample analysis, surface geological mapping, well logs, and the geophysical surface data that are also analysed here (Rejeki et al., 2010). The lithological units were classified into petrophysical groups (PG), each assigned the average, PG-specific porosity value estimated from helium saturation studies of core samples (Intani et al., 2012). This 3D porosity model is used here as a structural reference model for the second set of the 3D joint inversions performed. Porosities from the original model were mapped onto the rectilinear mesh used for 3D inversion modelling, extrapolated to cover the entire mesh, and smoothed (Figure 2).

Relating physical rock properties

While some geophysical parameters are readily linked via physical rock attributes – in particular density and porosity, favouring joint seismic and gravity inversion workflows – the relationships between other attributes are more complicated.

Electrical resistivity in geothermally prospective areas is controlled primarily by unrelated phenomena: conduction via interconnected pore fluids (in turn varying with salinity), alteration mineralogy, and clay-bounded water. In settings such as the Darajat field, low-resistivity zones are associated with relatively low-temperature clay alteration (presence of smectite). Shallow high resistivity indicates the absence of clay (e.g. unaltered near-surface lavas) in combination with dry and/or freshwater pore fluids, while the deeper, hotter, and more resistive reservoir zone is associated with less conductive clays (illite and chlorite)

and effective porosity is not high enough to generate low bulk resistivities. There are no direct physical relationships between electrical resistivity and seismic velocity or density, and therefore it is not possible to set direct links between these geophysical properties. (There have, however, been efforts using empirically derived statistical relationships between electrical resistivity and seismic velocity from well logs — see, for example, Chen and Hoversten, 2012.)

A cross-gradient joint inversion approach was followed here, therefore, to structurally link different geophysical domains, and subsequently the geophysical parameters to the reference porosity model, adding the respective cross-gradient terms to the objective function of the inversion, to be minimized within the course of the inversion (Gallardo and Meju, 2003; Scholl et al., 2017). Multiplicative factors set the balancing weight of these links with respect to the other terms of the function that measure data misfit and property structure.

The cross-gradient regularization supports structural similarity by measuring the norm of the vector product of the gradients of the involved properties. *Parallel as well as anti-parallel* gradients have no contribution and are therefore encouraged.

3D inversion modelling

All modelling was carried out using CGG's RLM-3D inversion suite, with 3D solvers for frequency-domain electromagnetic induction (MT, marine Controlled-Source EM, airborne AFMAG — Audio-Frequency MAGnetic EM), gravity and gravity gradiometry, and seismic traveltimes. Property regularization follows a minimum-structure approach (Tikhonov and Arsenin, 1977) and the objective function is minimized using a non-linear conjugate gradients scheme as described by Rodi and Mackie (2001).

MT forward modelling is based on the finite integration technique (Weiland, 1977) applied on orthogonal Cartesian grids (more details can be found in Mackie and Watts, 2012). The gravity simulation is based on the closed-form solutions for rectangular prisms found in Li and Chouteau (1998). Traveltimes are calculated using a CGG implementation of the FTeik3d code (Noble et al., 2012) solving the Eikonal equation through finite-difference approximations.

The standard approach to solving nonlinear geophysical inverse problems is by regularized least squares, in which the

solution is taken to be the minimum of an objective function of the form:

$$\Psi(\mathbf{m}) = (\mathbf{d} - F(\mathbf{m}))^T \mathbf{W}(\mathbf{d} - F(\mathbf{m})) + \lambda \mathbf{m}^T \mathbf{K} \mathbf{m},$$

where \mathbf{d} is the observed data vector, F is the forward modelling function, \mathbf{m} is the unknown model vector, \mathbf{W} is a weighting matrix (usually the inverse variance or covariance), λ is the regularization parameter, and \mathbf{K} is a discrete form of the stabilizing function. Additional terms may optionally measure deviations from an a priori model.

For joint inversions, the objective function is augmented to minimize the data misfits of more than one data type (here: two), the regularization of all model properties involved, and cross-gradient links between the properties. Labelling the data misfit and

model regularization terms Φ^{data} and Φ^{reg} , and cross-gradient terms between the model properties Φ^{cg} , the joint objective function can be rewritten as:

$$\Psi(\bar{\mathbf{m}}) = \sum_{j=1,2} \alpha_j \phi_j^{\text{data}} + \sum_{i=a,b} \lambda_i \phi_i^{\text{reg}} + \tau_{a,b} \phi_{a,b}^{\text{cg}} \left[+ \sum_{i=a,b} \tau_{i,\text{ref}} \phi_{i,\text{ref}}^{\text{cg}} \right],$$

where $\bar{\mathbf{m}}$ is an ensemble of model properties (a, b). Indices j refer to different data types. Factors α , λ , and τ weight the contribution of the respective terms to the objective function. For the data weights, the square root of the ratio between the total numbers of data points of the two methods involved is used (Commer and Newman, 2009).

Carefully edited MT impedance data were resampled to the 24 frequencies used in inversions, within 0.003 to 1800 Hz with four

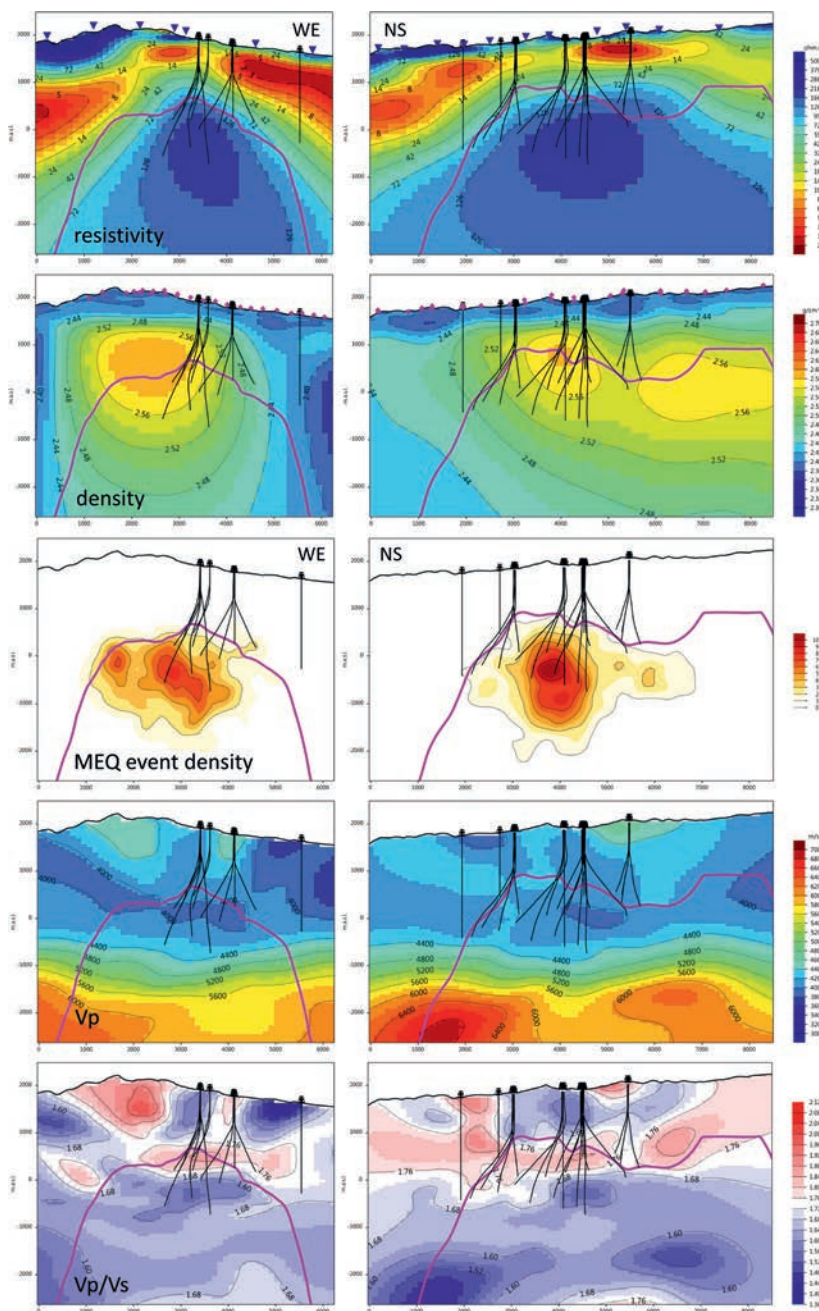


Figure 3 Results from single-domain 3D inversion of MT and gravity (resistivity and density, top rows), and from joint 3D seismic inversion (MEQ locations, shown as density plot in the centre, and Vp and Vs velocity, bottom rows), along profiles WE (left) and NS (right). The pink line marks the estimated top of the lava petrophysical group, as in Figure 2, added as reference.

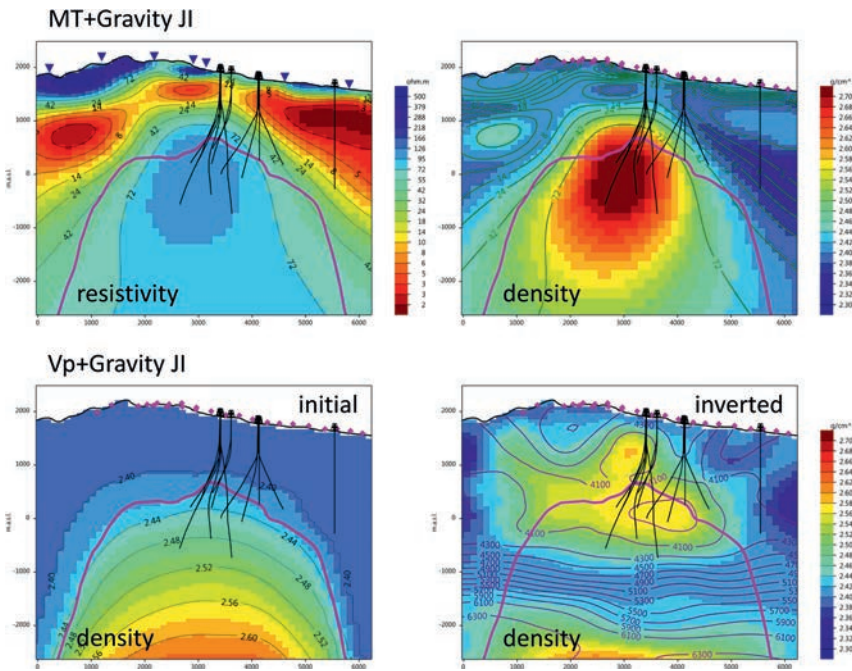


Figure 4 Joint inversion results without structural referencing to porosity, along Profile 'WE'. Top: resistivity and density from joint MT+gravity inversion. Coloured density to the right has resistivity contours superimposed, showing strong correlation. Both starting properties were homogeneous. Bottom: joint Vp+gravity inversion. The initial density model is shown to the left, and on inverted density to the right, Vp contours are superimposed, again demonstrating strong correlation. The estimated top of the lava petrophysical group is shown in pink.

frequencies per decade, and an error floor of 5% was used on all tensor components. Absolute densities were modelled, and free-air gravity was used as input to correctly model density variations in the near-surface. An absolute error of 0.5 mGal was assigned to the gravity data. MEQ seismic data were cleaned for outliers, and event locations near the lateral model bounds and outside an elevation range of -3500 to +500 m msl were removed. Results from initial 3D tomographic inversions – run separately for Vp and Vs – were used to further clean up the data set, excluding traveltimes with very high residuals. In this way, the MEQ data set was reduced to 5100 events, and 33,000 P- and S-wave arrivals. An error of 40 msec standard deviation was assigned to the traveltimes for inversion.

Single-domain and joint seismic inversions

Prior to the joint inversion analysis, blind single-domain inversions were performed for both MT and gravity. These inversions, besides serving as a final data quality control, helped to define appropriate inversion parameters such as data errors and regularization weights. Modelled structures provide direct indications on the specific data content, without contributions from other disciplines. The starting resistivity and density models were homogeneous: 50Ωm and 2.40g/cc respectively. Modelled resistivity shows a clear updoming of the deep resistor, with a shallower and thinner low-resistivity clay cap in the central producing zone (Figure 3). A density high is modelled at a similar location laterally, but its depth is controlled largely by the density inversion regularization.

In a different inversion run, MEQ tomography data were inverted jointly. Traveltimes were inverted for slowness of P and S waves, and event locations. The link between Vs and Vp velocity was established via cross-gradients. Initial models had vertically increasing velocity obtained from 1D inversion of P arrivals, and a constant initial Vp/Vs ratio of 1.75 was used. Inverted Vp velocity largely maintains the vertical trend of the starting model, but with significant spatial variation added (Figure 3). The Vp/Vs ratio reflects much of the structure in Vp,

with a largely positive correlation, i.e. zones of high Vp have mostly high Vp/Vs, and vice-versa. At an elevation of around 500m msl, Vp/Vs has a relative high, decreasing to a relative low in the production zone underneath.

Inter-discipline joint 3D inversions

Joint 3D inversions across disciplines were initially run without reference to the porosity model; MT+gravity and Vp+gravity inversion results are illustrated in Figure 4. For the MT+gravity inversion, starting properties were homogeneous, as in the single-domain inversions. The cross-gradient link introduced a strong correlation of gravity with resistivity, while changes in resistivity with respect to the single-domain inversion are minor in comparison. Note that the correlation is both positive (deep high resistivity = density high) and negative (outer resistivity minima = relative density highs) as per the design of the cross-gradient approach.

Also for the Vp+gravity inversion, the starting Vp model was a 1D gradient, as in the joint MEQ tomography. Initial density, however, had a gradual increase from 2.40 to 2.70 g/cc inserted beneath the estimated top lava flows horizon (Figure 4). In the inversion result, the strong vertical gradient in Vp velocity introduced a break in the initial continuous density increase with depth.

Successively, an additional cross-gradient link to porosity from the current geological model was used in the inversions to promote structural similarity (Figure 5). Modelled results clearly illustrate the linking between all three properties involved (Figure 6). The MT+gravity inversion started from the joint inversion result that did not involve a porosity link. Inverted density was edited by inserting a smooth gradient to a higher density of 2.7 g/cc within the lava petrophysical group, as considered more realistic – similar to the starting density used in the Vp+gravity inversions. Modelled resistivity maintains its structural characteristic, but adjusts locally to align with porosity contours.

In the joint MEQ+gravity inversion, starting properties were as in the joint inversion without the link to porosity. Inverted velocities agree with those of the tomographic joint inversion. However, the deep high velocity is more attenuated. The inverted density structure is notably consistent with the joint MT+gravity inversion.

Discussion

A key measure of the plausibility of the results from the joint inversions is how well they represent the ‘actual’ subsurface conditions. Interpretations of resource potential and size for exploration

and development targeting typically rely heavily on the resistivity models resulting from 1D, 2D or 3D MT interpretations.

Shown on Figure 7 to the left are the modelled resistivities at a constant depth of 400 m below the surface, from the joint MT+gravity 3D inversion with structural constraint from cross-gradients to porosity. The contours on the figure are the methylene blue percentages observed from drill cuttings (e.g. Gunderson et al., 2000). This depth slice is within the clay cap for the reservoir. Higher methylene blue percentages correspond to increased smectite and therefore lower resistivities. The

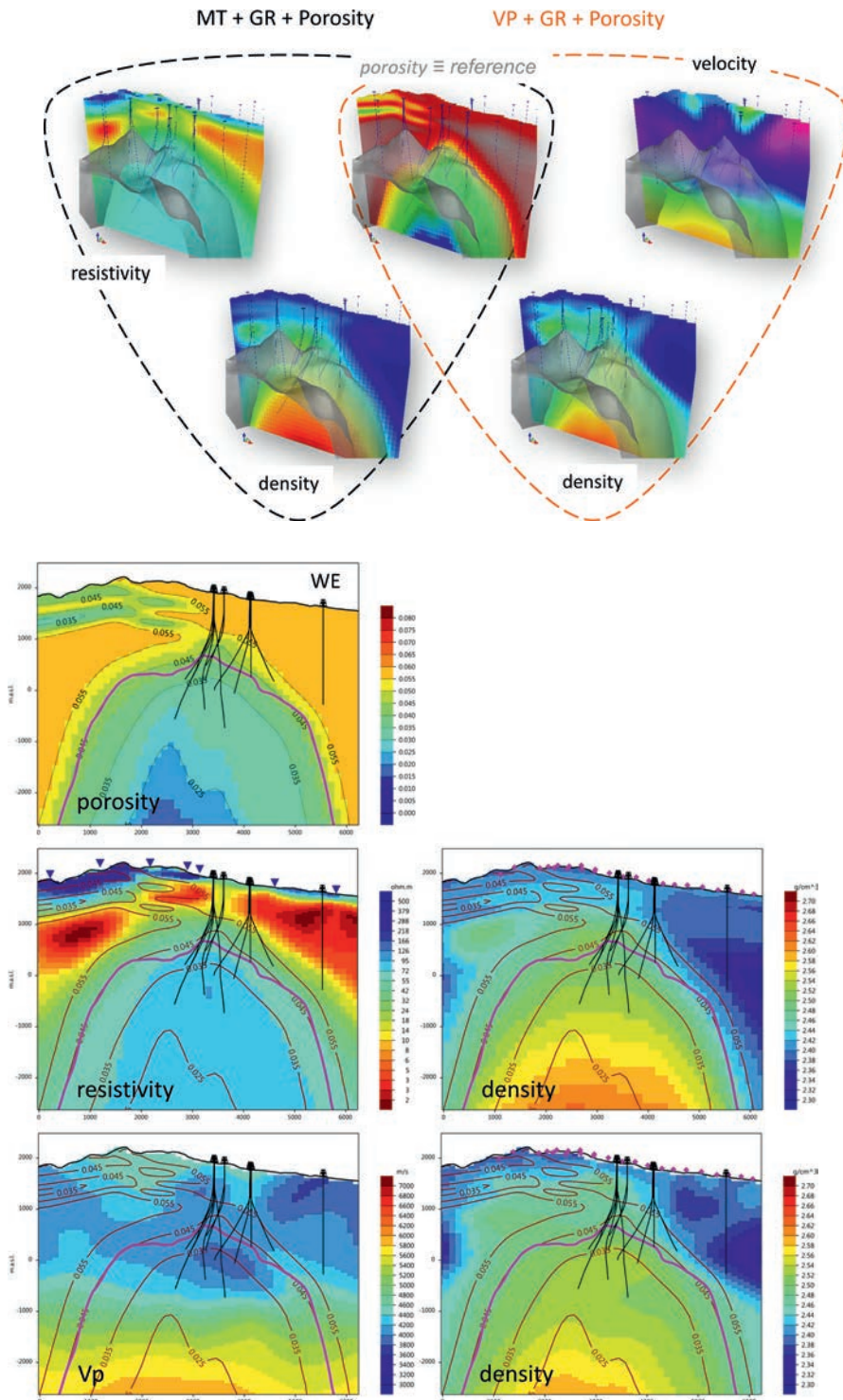


Figure 5 Joint inversions using cross-gradients to porosity. Inversion for resistivity and density (left), and velocity and density (right). In both cases, the porosity model was used as a structural reference model. All cross-property linking was via cross-gradients. The transparent surface marks the estimated top lava flows estimate as per Figure 2.

Figure 6 Joint inter-disciplinary 3D inversion results applying structural referencing to porosity via cross-gradients. Top row shows porosity section along profile ‘WE’. Centre: joint MT+gravity inversion results. Bottom: Vp+gravity inversion results. Porosity contours are superimposed on all inverted properties for comparison. The estimated top of the lava petrophysical group is shown in pink.

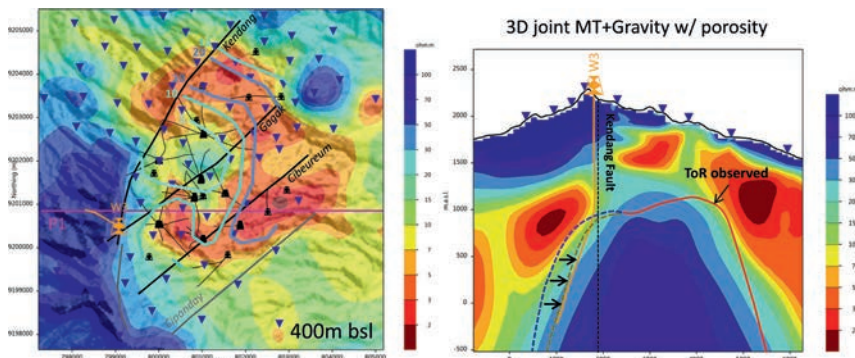


Figure 7 Resistivity from MT+gravity inversion, applying structural referencing to porosity via cross-gradients (coloured grids). Left: constant depth slice at 400 m from the surface. Contours are a percentage of methylene blue, higher values indicating increased smectite. Right: section along profile P1, plotted with a vertical exaggeration of two. Top of Reservoir (ToR) in the drilled portion of the reservoir is shown with a solid red line. The interpreted potential extension of the ToR prior to drilling of well W3 is shown as a dashed blue line. The joint 3D inversion suggests a narrower extension as indicated with the dashed brown line.

spatial distribution of the resistivity from the joint inversion result matches these contours closely and is thus expected to represent the smectite trends and changes in the clay cap well.

The true value of joint 3D inversion, however, comes into play at deeper levels. During the last drilling campaign in Darajat (2009-2011) one of the wells (W3) was targeted west of the Kendang fault to test for a possible extension of the reservoir (Intani et al., 2015). The targeting was justified based on an integrated interpretation which relied heavily on the interpretation of the standalone resistivity modelling.

The right of Figure 7 shows a resistivity section along west-east Profile P1 from the same joint 3D MT+gravity inversion. The figure shows the Top of Reservoir (ToR) where it was drilled (solid red line) and the interpreted potential extension west of the Kendang fault based on the geometry of the low-resistivity clay cap (dashed blue line) prior to drilling well W3. From the then available 1D Occam resistivity models, it was interpreted that there was a good chance that the reservoir could extend well west of the fault, and W3 was subsequently targeted to test this interpretation. Post-drilling results, however, showed sub-commercial temperatures and permeabilities, indicating the reservoir margin in this area of the field is likely to be bounded by or near to the Kendang fault (Intani et al., 2015), as is accurately predicted by the joint 3D modelling results presented here: the margin of the ToR would be interpreted to be very near W3-targeted TD. Resistivity from the 3D joint inversion has an improved resolution of the low resistivities that cap the reservoir, especially near the margins where the details of thickness and depth of the low resistivity base are of key importance in the interpretation of reservoir extent.

The relatively lower V_p extending into the lower-porosity and higher-density lava formation (Figure 6) was initially a surprise. However, on further reflection, this is expected. Here, fracture density in the geothermal system's naturally fractured reservoir (NFR) is increased. Wave velocity decreases as fracture density increases, as the fluid phase changes from liquid to steam in the matrix pore space, and as pressure and temperature decrease (e.g. O'Connell and Budiansky, 1974). Impacts from production that could locally lower V_p are also expected given the inverted MEQ data set spans the steam production period.

These new results should help in the targeting of development wells and potential step-out wells. For example, the higher density/resistivity lavas are found to host more permeable entries than the other formations (Intani et al., 2017). Improved confidence in the location of these formations, particularly away from existing wells, will be an important consideration in the next drilling campaign.

Conclusions

3D joint inversion modelling resulted in mutually consistent resistivity, density and velocity models. Structural referencing to porosity via cross-gradients to a 3D porosity volume from a geological model was tested and showed the consistency of modelled structure with the current geological understanding of the field. With respect to the single-domain runs, the joint-domain inversions provide more reliable structural images of both the low-resistivity clay cap, and the resistive reservoir region beneath.

Updating the working geothermal system model through 3D cross-gradient joint inversions of the MT, gravity and MEQ data sets has provided reliable targeting of future step-out development wells at the reservoir margins. Comparison of the joint MT resistivity model with previous modelling across an area targeted for step-out drilling in the NW portion of the field showed the joint model was more representative. The improved resolution from the joint inversion models also provides better well targeting of permeable entries.

The work was carried out in close collaboration with the Darajat asset development team (Star Energy Geothermal) to ensure rigorous assessment of results in the light of Darajat's 30-year plus exploration and production history. We expect that similar joint inversion workflows employed both early in and during the lifetime of the field would strengthen the building of a concept model for exploration, and that later updates would guide development drilling programmes.

References

- Chen, J. and Hoversten, G.M. [2012]. Joint inversion of marine seismic AVA and CSEM data using statistical rock-physics models and Markov random fields. *Geophysics*, **77**, R64-R80.
- Commer, M. and Newman, G.A. [2009]. Three-dimensional controlled-source electromagnetic and magnetotelluric joint inversion. *Geophysical Journal International*, **178**, 1305-1316.
- Cumming, W. [2009]. Geothermal resource conceptual models using surface exploration data. *34th Workshop on Geothermal Reservoir Engineering*, SGP-TR-187.
- Gallardo, L.A. and Meju, M.A. [2003]. Characterization of heterogeneous near-surface materials by joint 2D inversion of DC resistivity and seismic data. *Geophysical Research Letters*, **30**, 1658.
- Gunderson, R., Cumming, W., Astra, D., and Harvey, C. [2000]. Analysis of smectite clays in geothermal well cuttings by the Methylene Blue Method: For well site geothermometry and resistivity sounding correlation. *World Geothermal Congress*, Extended Abstracts.

- Intani, R.G., Fitriyanto, A., Mahagyo, P., Golla, G., Irfan, R. and Waite M. [2012]. Overview of the 2012 Darajat 3D earth model. *12th Annual Indonesian Geothermal Association Meeting and Conference*, Extended Abstracts.
- Intani, R.G., Simatupang, C., Sihombing, A., Irfan, R., Golla, G. and Pasaribu, F. [2015]. West edgefield evaluation of the Darajat geothermal field, Indonesia. *World Geothermal Congress*, Extended Abstracts.
- Intani, R.G., Satya, D.Y., Golla, G. and Nordquist, G. [2017]. Permeable entry characterization at Darajat geothermal field, West Java. *5th Indonesian Annual Geothermal Convention and Exhibition*, Extended Abstracts.
- Li, X. and Chouteau, M. [1998]. Three-dimensional gravity modeling in all space. *Surveys in Geophysics*, **19**, 339-368.
- Mackie, R.M. and Watts, M.D. [2012]. Detectability of 3-D sulphide targets with AFMAG. *SEG Technical Program*, Expanded Abstracts, **257**, 1-4. doi: 10.1190/segam2012-1248.1.
- Noble, M.S., Gesret, A. and Belayouni, N. [2012]. New 3D Eikonal solver for accurate traveltimes, takeoff angles and amplitudes. *74th EAGE Conference & Exhibition incorporating EUROPEC 2012*, Extended Abstracts.
- O'Connell, R.J. and Budiansky, B. [1974]. Seismic velocities in dry and saturated cracked solids. *Journal of Geophysical Research*, **79**, 5412-5426.
- Perdana, M.W. and Nelson, C. [2014]. Microseismic monitoring in Darajat geothermal field: Observations in moving injection to DRJ-AI well. *Indonesia International Geothermal Convention & Exhibition*, Jakarta, Extended Abstracts.
- Pramono, B. and Colombo, D. [2005]. Microearthquake characteristics in Darajat geothermal field, Indonesia. *World Geothermal Congress*, Extended Abstracts.
- Rejeki, S., Rohrs, D., Nordquist, G. and Fitriyanto, A. [2010]. Geologic conceptual model update of the Darajat geothermal field, Indonesia. *World Geothermal Congress*, Extended Abstracts.
- Rodi, W. and Mackie, R.L. [2001]. Nonlinear conjugate gradients algorithm for 2D magnetotelluric inversion. *Geophysics*, **66**, 174-187.
- Scholl, C., Hallinan, S., Watts M.D. and Miorelli, F. [2017]. Geological consistency from inversions of geophysical data. *79th EAGE Conference & Exhibition*, Extended Abstracts.
- Soyer, W., Mackie, R., Hallinan, S., Pavesi, A., Nordquist, G., Suminar, A., Intani, R. and Nelson, C. [2017]. Multi-physics imaging of the Darajat field. *Geothermal Resources Council Annual Meeting*, Transactions, **41**, 1724-1741.
- Tikhonov, A.N. and Arsenin, V.Y. [1977]. *Solutions of ill-posed problems*. V. H. Winston and Sons.
- Trainor-Guitton, W.J., Hoversten, G.M., Ramirez, A., Juliusson, E., Mellors, R. and Roberts, J. [2014]. Value of information using calibrated geothermal field data. *39th Workshop on Geothermal Reservoir Engineering*, Extended Abstracts, SGP-TR-202.
- Ussher, G., Harvey, C., Johnstone, R. and Anderson, E. [2000]. Understanding the resistivities observed in geothermal systems. *Proceedings World Geothermal Congress*, Extended Abstracts.
- Weiland, T. [1977]. A discretization method for the solution of Maxwell's equations for six-component fields. *Electronics and Communications AEU*, **31**, 116-120.

ADVERTISEMENT



Game changing OBN efficiency. Delivered.

inApril

www.inapril.com

Please visit us at EAGE Copenhagen, Booth 1111